MR NORBERT CALDERA (Orcid ID : 0000-0002-2383-4097)

Article type : Review Article

Recumbent folding in the Upper Cretaceous Eaux-Chaudes massif: a Helvetic-type nappe in the Pyrenees?

Norbert Caldera[1], Antonio Teixell[1], Albert Griera[1], Pierre Labaume[2] and Abdeltif Lahfid[3]

[1]Departament de Geologia, Universitat Autònoma de Barcelona, 08193 Bellaterra (Barcelona), Spain

[2] Géosciences Montpellier, Université de Montpellier, CNRS, Université des Antilles, 34095 Montpellier, France

[3] Bureau de Recherches Géologiques et Minières, Orléans, France

Corresponding author: Norbert Caldera (email: norbert.caldera@uab.cat)

Significance statement: The Pyrenean orogenic deformation is most often characterized by thrust-fold systems formed under brittle conditions. The Eaux-Chaudes massif is an inlier of Upper Cretaceous sediments within the hinterland Axial Zone of the Pyrenees which allows to characterize the post-Variscan structure in this basement massif. Here we report for the first-time a recumbent fold structure, developed under ductile conditions in the Upper Cretaceous carbonates, with upper Paleozoic metasediments in the core. The fold nappe displays a km-scale, large overturned limb affected by high non-coaxial deformation (mylonitic fabric and strong crystallographic preferred orientation of calcite). Recorded paleotemperatures >300ºC in the Upper Cretaceous rocks are consistent with the microstructure observed. This is a novel deformation style previously unreported for the

alpine Pyrenees, comparable with other analogues as for example the lower Helvetic nappes of the Alps.

The results reported in the manuscript are of broaden general interest, especially for the community focused on mountain building processes, and provide a unique example to decipher the thermomechanical evolution in complex hinterland areas, as the Axial Zone of the Pyrenees. Our interpretations are supported with new cartography and structural cross-section, paleotemperature using RSCM technique and microstructure analysis using SEM-EBSD.

Abstract

We describe a singular structure in Upper Cretaceous rocks of the Eaux-Chaudes massif of the western Pyrenees, consisting of a km-scale fold nappe with a sheared overturned limb. High ductile strain attests a deformation style rarely reported for the alpine Pyrenees, and peak temperature in Upper Cretaceous carbonates is estimated by RSCM paleothermometry in the lower greenschist facies (>300ºC). The normal fold limb retains the original sedimentary textures, while the overturned limb shows calcite crystal-plastic deformation and dynamic recrystallization, with crystallographic preferred orientation. The observed ductility and metamorphic temperature bear similarities with the lower Helvetic nappes of the Alps, suggesting deep burial and/or possibly high geothermal gradient in this part of the Pyrenees.

1 INTRODUCTION

In orogens formed by tectonic inversion, the reactivation of extensional structures and the formation of thrust-related basement uplifts commonly accommodate the compressional deformation (e.g. Lacombe & Bellahsen, 2016; Pfiffner, 2017; Herwegh et al., 2020). The interiors of basement uplifts are often poorly understood due to structural complexity and limited outcrops of post-basement rocks. This study focusses on the Axial Zone of the Pyrenees, an Alpine orogen resulting from the inversion of a Mesozoic hyperextended rift (Jammes et al., 2009; Lagabrielle et al., 2010; Masini et al., 2014; Teixell et al., 2016, 2018). The Pyrenees conform to an asymmetric doubly-verging wedge (Choukroune et al., 1989; Muñoz, 1992; Teixell, 1998) which formed from late Cretaceous to early Miocene times

(Alpine orogeny) (Fig. 1). The Axial Zone comprises a system of thrust sheets made of Iberian Paleozoic basement (previously deformed by the Variscan orogeny) which connects to a south-verging thin-skinned thrust system of Mesozoic and Tertiary rocks (South Pyrenean Zone). North of the Axial Zone, the North Pyrenean Zone (NPZ) comprises the inverted Mesozoic basin axis which overrides both the Aquitaine foreland by the North Pyrenean Frontal Thrust and the Axial Zone by the North Pyrenean Fault and the Lakora thrust (Muñoz, 1992; Teixell, 1998; Mouthereau et al., 2014; Teixell et al., 2016).

The Eaux-Chaudes massif (ECM) comprises an inlier of Upper Cretaceous rocks surrounded by Paleozoic rocks in the northwestern Axial Zone (Fig. 2). The massif has been classically interpreted as a duplex structure with a roof thrust carrying Paleozoic basement (Ternet, 1965; Déramond et al., 1985; Dumont et al., 2015). The Upper Cretaceous sedimentary cover constitutes a key-marker to constrain the structural style and paleotemperature conditions during the Alpine orogeny.

We present a novel view of the Eaux-Chaudes structure (Fig. 3), documented by structural mapping, microstructure and paleotemperature data, which highlights a kilometre-scale recumbent fold nappe. Our observations evidence the importance of alpine ductile folding not recognized hitherto in the hinterland of the Pyrenees.

2 TECTONIC SETTING

Paleotectonic reconstructions place the Upper Cretaceous platform carbonates of the ECM in the upper margin of the Iberian plate during the Mesozoic post-rift stage (e.g. Teixell et al., 2016 and references therein). These carbonates later became sandwiched between Paleozoic rocks during the Pyrenean convergence.

The Upper Cretaceous sequence lies unconformably on Silurian to Carboniferous metasedimentary rocks, mainly shales, limestones, and sandstones, and on the late Paleozoic Eaux-Chaudes granite. Occasionally lower Triassic Buntsandstein conglomerate pods are preserved in between the Paleozoic and the Upper Cretaceous (Ternet, 1965). The Cretaceous sequence consists of a lower unit of mudstones and grainstones (“Calcaires des Cañons”, Cenomanian to Santonian) followed by sandstone-shale Flysch of Campanian-Maastrichtian age (Ternet, 1965), a sequence which represents the early stages of

subsidence related to the Pyrenean orogeny (Teixell, 1993). Cenomanian-Turonian formations are discontinuous due to local erosion events, as observed elsewhere in the western Axial Zone (Souquet, 1967; Teixell et al., 1994). The ECM is overlain by the Lakora thrust complex (Fig. 2), here represented by Paleozoic (Montagnon d'Iseye thrust unit) and Upper Triassic rocks (mostly Keuper and ophites, Bedous unit), which is in turn overlain by the detached Jurassic-Lower Cretaceous rocks of the southern Chaînons Béarnais (Ternet et al. 2004, Labaume & Teixell, 2020). The whole system was uplifted in the hanging wall of the Gavarnie thrust that raised the Axial Zone, imparting local backthrusting deformation in the ECM (D2 in Dumont et al., 2015). Thrusting of the Lakora-Eaux-Chaudes units is attributed to the latest Cretaceous to mid-Eocene, while subsequent Gavarnie thrusting in the western Axial Zone is attributed to the late Eocene-early Oligocene (Teixell, 1996; Labaume et al., 2016).

3 METHODOLOGY

Field structural analysis and mapping was combined with cross-section construction to interpret the large-scale structure. Samples were analysed by thin section and scanning electron microscopy (SEM) coupled with electron backscattered diffraction (EBSD) and energy dispersive spectrometry (EDS). EBSD data were collected at the University of Montpellier on a CamScan Crystal Probe X500FE.

Raman spectroscopy of carbonaceous material (RSCM) was performed at the BRGM (Orléans) to calculate peak temperatures (T_{max}) using a diode-pumped solid-state laser source excitation of 514.5 nm. The laser power reaching the sample surface, through the 100x objective of a Leica DM2500 microscope, did not exceed 1 mW. We followed the procedures described by Beyssac et al. (2002, 2003, 2007) and Lahfid et al. (2010).

4 RESULTS

We propose a new structural profile of the ECM showing an unexpected large-scale ductile structure defined by the Upper Cretaceous rocks (Figs. 3, 4), consisting of a south-verging ~5km-long recumbent fold nappe cored by folded Silurian-Devonian metasediments with a near-horizontal axial plane and a large overturned limb. The Paleozoic core shows minor folds with subhorizontal axial planes and heterogeneously distributed foliation. The

overturned limb is in thrust contact over an autochthonous panel of weakly deformed Upper Cretaceous carbonates (Figs. 2, 3, 4). Occasional Keuper and ophite slices are found along the contact (Ternet, 1965). The Eaux-Chaudes recumbent structure shows an immersion to the west, consistent with the regional plunge of the western Axial Zone, and hence it disappears laterally below overlying thrust sheets. East of the Ossau valley it is largely eroded, so the valley area provides a unique opportunity to observe the proposed structural relationships.

Sample analyses were performed in the Upper Cretaceous of the autochthon, the overturned limb and the normal limb of the fold nappe (Figs. 3, 4).

4.1 Structural analysis

In the Upper Cretaceous of the autochthonous and normal-limb domains, sedimentary textures are preserved, despite small-scale brittle faults, and a spaced pressure-solution cleavage. Generally, fossils are unstrained apart from solution seams, and ductile deformation at the grain scale is not observed. EBSD analysis of calcite aggregates show random distribution of crystallographic a-, m- and c-axes (Fig. 5). The average grain size is ~32 μm, ranging between 16-100 μm. Occasionally, deformation twins of type III-IV (Ferrill et al., 2004) are observed in coarser calcite grains.

The overturned limb is characterized by strong ductile deformation that obliterates fossil content. It shows a mylonitic foliation subparallel to bedding at the mesoscale, and stretching lineation, both inclined to the north (Fig. 5). Microfabrics are controlled by the rheological behaviour of the mineral phases. In calcite-rich layers, crystal-plastic deformation is dominant with development of a fine-grained matrix (9-28 μm, decreasing grain size with increasing deformation intensity) featuring grain-shape preferred orientation and S-C composite fabrics (Fig. 5). We observed evidence of grain boundary migration, such as lobate and interfingering grain boundaries and subgrains. Well-developed CPO is recorded, with c-axes oriented normal to the foliation, and a- and m- axes defining a girdle parallel to the foliation (Fig. 5). Aligned oxide minerals (<1 vol%) parallel to the main foliation enhance the anisotropic fabric. Thin dolomite-rich layers are observed in some samples. These layers show moderate plastic deformation, with occasional fold streaks and asymmetric

porphyroclasts (Fig. 6). Quartz- and phyllosilicate-rich layers (e.g. Buntsandstein and Cretaceous clastic limestones) show brittle-to-ductile behaviour, with weak intragranular deformation (undulose extinction) and slight evidence of quartz recrystallization by bulging. S-C fabrics and asymmetric porphyroclasts attest a non-coaxial deformation and evidence the south-directed tectonic transport previously reported by Ternet (1965), Majesté-Menjoulas (1979), Dumont et al. (2015) and Cochelin (2016). Microstructure and EBSD of monomineralic calcite aggregates suggest plastic deformation by dislocation creep accommodated by slip on basal planes parallel to the a- and m-axes.

4.2 RSCM paleothermometry

Raman Spectroscopy of Carbonaceous Material is based on the analysis of the degree of structural organization of carbonaceous material (CM) as a proxy for the T_{max}. CM structure is not sensitive to retrograde transformations, remaining on the maximum temperature reached during metamorphism (Beyssac et al., 2002). Raman spectra are composed in the first region (Tuinstra & Koenig, 1970; Nemanich & Solin, 1979) by the graphite band (G) and defect bands ($D_{1\text{-}4}$).

The spectra from the autochthonous and overturned limb were fitted by the Beyssac et al. (2002) method, since it is well adapted to the temperature range 320-650ºC. Samples from the normal limb best fittings were obtained by the method of Lahfid and others (2010), which works better in the temperature range 150-320ºC. In either case, T_{max} values obtained for all samples range between 315-350ºC (Fig. 7 and Table 1). Representative Raman spectra (Fig. 7) from the undeformed autochthonous unit and overturned limb show differences between the intensities of D1 and G bands with D1 band more intense. This indicates a temperature higher than 330ºC. In the normal limb, both D1 and G bands show a very similar intensity, implying a lower temperature of approximately 315ºC.

5 DISCUSSION

The ECM represents the inverted Iberian rifted margin where Upper Cretaceous rocks have been ductilely folded. Large-scale recumbent folding is accompanied by high-strain shearing in the overturned limb, with extensive crystal-plastic deformation and

recrystallization, not reported hitherto for the compressional deformation of the post-Paleozoic rocks of the Pyrenees.

The Pyrenean Axial Zone is interpreted as a stack of basement units buried and deformed during the Cenozoic at temperatures in general <300ºC (e.g. Fitzgerald et al., 1999; Jolivet et al., 2007; Metcalf et al., 2009; Abd Elmola et al., 2017; Bellahsen et al., 2019). This work shows for the first-time evidence for ductile basement-involved thin-skinned deformation (i.e. Pfiffner, 2017) in the Pyrenees, affecting the upper Paleozoic metasediments and the overlying Mesozoic sedimentary rocks. RSCM geothermometric results for the Jurassic-Lower Cretaceous rocks of the NPZ in the vicinity are in a range of 300-400ºC (Clerc et al., 2015; Corre, 2017). However, this metamorphic peak is associated with the mid-Cretaceous episode of crustal hyperextension in the Pyrenean rift (Golberg & Leyreloup, 1990; Clerc & Lagabrielle, 2014; Saspiturry et al., 2020), and not with the Alpine orogeny as in the Upper Cretaceous at Eaux-Chaudes. The microstructural features observed at ECM are consistent with the RSCM estimates. Type IV deformation twins are indicative of temperatures >250ºC (Ferrill et al., 2004), complete recrystallization of calcite is commonly reported at temperatures >300ºC (Weber et al., 2001), and incipient bulging recrystallization in quartz is documented for the range 300-400ºC (Stipp et al., 2002).

Our proposed cross-sectional geometry differs notably from previously published structural interpretations (Ternet, 1965; Déramond et al., 1985; Dumont et al., 2015; Cochelin, 2016). The recumbent fold poses the question of the mechanical behaviour of the Paleozoic metasediments located in the deformed core of the structure. The bulk of these rocks is rich in phyllosilicates, i.e. slates with limestone and sandstone intercalations of Devonian age, and graphitic Silurian slates. The main foliation observed in these rocks is consistent with the large structure, although could partly derive from an earlier Variscan fabric (Dumont et al., 2015; Cochelin, 2016) that was reworked during Alpine deformation. Mapping suggests that the Eaux-Chaudes fold nappe was detached in the weak Silurian rocks. The contact that is usually mapped as the Eaux-Chaudes thrust in the Ossau valley (e.g. Ternet et al., 2004) is here reinterpreted as an overturned stratigraphic boundary between Paleozoic and Upper Cretaceous carbonates, supported by (1) the occurrence of

overturned Buntsandstein pods along the contact, (2) a large-scale folded Paleozoic stratigraphy cored by Silurian slates, and (3) the recognition by Ternet (1965) of an overturned panel involving Paleozoic and Cretaceous rocks at Bouerzy and Cézy peaks (Fig. 2) in the hinge of the structure. Along the Ossau valley, the highly-deformed Upper Cretaceous carbonates of the overturned limb are in sharp contact with the low deformed and sub-horizontal autochthonous Upper Cretaceous carbonates (Figs. 3, 4). The Keuper and ophite bodies along the contact may represent relicts of the Triassic sole of the overlying Lakora thrust sheet, squeezed out from the faulted (welded) synform during recumbent folding (Fig. 8).

This Pyrenean structure has similarities to the lower Helvetic Morcles-Doldenhorn nappes of the Alps, which are recumbent folds with long overturned limbs involving low-grade Mesozoic metasedimentary rocks (e.g. Ramsay, 1981; Burkhard, 1988; Pfiffner, 1993; Casey & Dietrich, 1997; Herwegh & Pfiffner, 2005). Paleotemperature data (315-350ºC), grain size (9-28 μm) and microstructure (dislocation creep-induced textures, dynamic recrystallization and associated grain size reduction) are also comparable. For example, Austin et al. (2008) reported average grain size between 7-22 μm for samples deformed in a temperature range 337-358ºC in the Morcles Nappe. Similar grain sizes and paleotemperatures were also reported for the Doldenhorn and Glarus nappes by Herwegh & Pfiffner (2005) and Ebert et al. (2007, 2008).

A challenge resides in explaining the high temperatures recorded by the Upper Cretaceous rocks in the ECM. In the Helvetic case, high temperature can be explained by tectonic burial by the overlying Penninic and Austroalpine nappes, with a structural pile >15 km (Dietrich & Casey, 1989; Pfiffner et al., 1997; Herwegh & Pfiffner, 2005; Nibourel et al., 2018). Such deep burial is more difficult to envisage for the Pyrenees where the thrust stack is considered much thinner (e.g. Teixell, 1998; Bellahsen et al., 2019). The measured ~30ºC difference between the normal and overturned limbs at Eaux-Chaudes, for samples ~1 km apart vertically, could indicate a normal geothermal gradient in the fold domain, although this difference lies within the RSCM error margins and, therefore, cannot be conclusive. A 30ºC/km gradient for the Iberian margin is near to the 34ºC/km gradient estimated for the

European conjugate margin by Saspiturry et al. (2020). However, a 30ºC/km gradient would imply ~11 km of burial over the fold nappe, which is hard to reconcile with the tectonic pile that can be reconstructed above (Labaume & Teixell, 2020). Labaume et al. (2016), based on thermochronology-assisted restoration, estimated ~8 km of total burial over the Eaux-Chaudes thrust units (including synorogenic Flysch), representing a 40ºC/km gradient using our paleotemperatures. The available observations cannot unequivocally discriminate between deep burial or high geothermal gradient, the latter a relict of the Mesozoic thinning phase as proposed by Bellahsen et al. (2019) for other parts of the Iberian paleomargin in the Axial Zone.

6 CONCLUSIONS

We propose a novel structural interpretation for the Upper Cretaceous of the Eaux-Chaudes massif with a style reported for the first time in post-Paleozoic rocks of the Pyrenees. It consists of a large recumbent fold nappe, cored by Paleozoic phyllosilicate-rich metasediments and comprising a km-long overturned and sheared limb, showing similarities with the fold nappes of the lower Helvetic Alps.

According to RSCM paleothermometry, the Upper Cretaceous carbonates of the Eaux-Chaudes nappe reached the lower greenschist facies with peak temperature of ~350ºC. Mylonitic foliation and stretching lineation are well-developed in the overturned fold limb. Crystallographic and shape-preferred orientations in calcite are consistent with plastic deformation and extensive dynamic recrystallization indicating top-to-the-south shear sense. These observations evidence a high temperature of the Axial Zone during Alpine deformation and rends challenging its interpretation between a deep burial and/or a high geothermal gradient relict from the Mesozoic thinning phase.

ACKNOWLEDGMENTS

This work was supported by the Spanish MINECO/MCIU projects CGL2014-54180 and PGC2018-093903-B-C21. We thank the OROGEN project for enabling the acquisition of RSCM data, cofounded by Total S.A., BRGM and Institut national de sciences de l'Univers (INSU). Fabrice Barou is thanked for EBSD acquisition assistance and data treatment at

Géosciences Montpellier. We thank T. Dumont, D. Westerman, B. Cochelin and anonymous reviewers for comments that helped to improve the original manuscript.

DATA AVAILABILITY STATEMENT

The data that support the findings of this study are available from the corresponding author upon a reasonable request.

CONFLICT OF INTEREST: None.

REFERENCES CITED

Abd Elmola, A., Charpentier, D., Buatier, M., Lanari, P. & Monié, P. (2017). Textural-chemical changes and deformation conditions registered by phyllosilicates in a fault zone (Pic de Port Vieux thrust, Pyrenees). *Applied Clay Science, 144*, 88-103. https://doi.org/10.1016/j.clay.2017.05.008

Austin, N., Evans, B., Herwegh, M. & Ebert, A. (2008). Strain localization in the Morcles nappe (Helvetic Alps, Switzerland). *Swiss Journal of Geosciences, 101*, 341-360. https://doi.org/10.1007/s00015-008-1264-2

Bellahsen, N., Bayet, L., Denele, Y., Waldner, M., Airaghi, L., Rosenberg, C., Dubacq, B., Mouthereau, F., Bernet, M., Pik, R., Lahfid, A. & Vacherat, A. (2019). Shortening of the axial zone, Pyrenees: Shortening sequence, upper crustal mylonites and crustal strength. *Tectonophysics, 766*, 433-452. https://doi.org/10.1016/j.tecto.2019.06.002

Beyssac, O., Goffé, B., Chopin, C. & Rouzaud, J.-N. (2002). Raman spectra of carbonaceous material in metasediments: A new geothermometer. *Journal of Metamorphic Geology, 20*, 859-871. https://doi.org/10.1046/j.1525-1314.2002.00408.x

Beyssac, O., Goffé, B., Petitet, J.-P., Froigneux, E., Moreau, M. & Rouzaud, J.-N. (2003). On the characterization of disordered and heterogeneous carbonaceous materials by Raman spectroscopy. *Spectrochimica Acta Part A: Molecular and Biomolecular Spectroscopy, 59*, 2267-2276. https://doi.org/10.1016/S1386-1425(03)00070-2

Beyssac, O., Simoes, M., Avouac, J. P., Farley, K. A., Chen, Y.-G., Chan, Y.-C. & Goffé, B. (2007). Late Cenozoic metamorphic evolution and exhumation of Taiwan. *Tectonics, 26*. https://doi.org/10.1029/2006TC002064

Burkhard, M. (1988). L'Helvetique de la bordure occidentale du massif de l'Aar (evolution tectonique et métamorphique). *Eclogae geologicae Helvetiae, 81,* 63-114.

Casey, M. & Dietrich, D. (1997). Overthrust shear in mountain building. In: Sengupta S. (eds) *Evolution of Geological Structures in Micro- to Macro-scales,* 119-142. Springer. https://doi.org/10.1007/978-94-011-5870-1_8

Choukroune, P., and ECORS Team. (1989). The ECORS deep seismic profile reflection data and the overall structure of an orogenic belt. *Tectonics, 8*, 23-29.

Clerc, C. & Lagabrielle, Y. (2014). Thermal control on the modes of crustal thinning leading to mantle exhumation: Insights from the Cretaceous Pyrenean hot paleomargins. *Tectonics, 33*, 1340-1359. https://doi.org/10.1002/2013TC003471

Clerc, C., Lahfid, A., Monié, P., Lagabrielle, Y., Chopin, C., Poujol, M., Boulvais, P., Ringenbach, J. C., Masini, E. & de St Blanquat, M. (2015). High-temperature metamorphism during extreme thinning of the continental crust: A reappraisal of the North Pyrenean passive paleomargin. *Solid Earth, 6*, 643-668. https://doi.org/10.5194/se-6-643-2015

Cochelin, B. (2016). Champ de deformation du socle paléozoïque des Pyrénées. *Sciences de la Terre. Université Toulouse 3 Paul Sabatier (UT3 Paul Sabatier). Français.*

Corre, B. (2017). La bordure nord de la plaque Ibérique à l'Albo-Cénomanien. Architecture d'une marge passive de type ductile (Chaînons Béarnais, Pyrénées Occidentales). *Sciences de la Terre. Université Rennes 1, PhD thesis*. France.

Déramond, J., Graham, R., Hossack, H., Baby, J. R., Crouzet, P. & Crouzet, G. (1985). Nouveau modéle de la chaîne des Pyrénées. *Comptes Rendus de l'Académie des Sciences, Paris, 301*, 1213-1216.

Dietrich, D. & Casey, M. (1989). A new tectonic model for the Helvetic nappes. *Geological Society, London, Special Publications, 45*, 47-63. https://doi.org/10.1144/GSL.SP.1989.045.01.03

Dumont, T., Replumaz, A., Rouméjon, S., Briais, A., Rigo, A. & Bouillin, J.-P. (2015). Microseismicity of the Béarn range: Reactivation of inversion and collision structures at the northern edge of the Iberian plate. *Tectonics, 34*, 934-950. https://doi.org/10.1002/2014TC003816

Ebert, A., Herwegh, M., Evans, B., Pfiffner, A., Austin, N. & Vennemann, T. (2007). Microfabrics in carbonate mylonites along a large-scale shear zone (Helvetic Alps). *Tectonophysics, 444*, 1-26. https://doi.org/10.1016/j.tecto.2007.07.004

Ebert, A., Herwegh, M., Berger, A. & Pfiffner, O. A. (2008). Grain coarsening maps for polymineralic carbonate mylonites: a calibration based on data from different Helvetic nappes (Switzerland). *Tectonophysics, 457*, 128-142. https://doi.org/10.1016/j.tecto.2008.05.007

Ferrill, D. A., Morris, A. P., Evans, M. A., Burkhard, M., Groshong Jr., R. H. & Onasch, C. M. (2004). Calcite twin morphology: a low-temperature deformation geothermometer. *Journal of Structural Geolgoy, 26 (8)*, 1521-1529. https://doi.org/10.1016/j.jsg.2003.11.028

Fitzgerald, P. G., Muñoz, J. A., Coney, P. J. & Baldwin, S.L. (1999). Asymmetric exhumation across the Pyrenean orogen: implications for the tectonic evolution of a collisional orogen. *Earth and Planetary Science Letters, 173 (3)*, 157-170. https://doi.org/10.1016/S0012-821X(99)00225-3

Golberg, J. M. & Leyreloup, A. F. (1990). High temperature-low pressure Cretaceous metamorphism related to crustal thinning (Eastern North Pyrenean Zone, France). *Contributions to Mineralogy and Petrology, 104*, 194-207. https://doi.org/10.1007/BF00306443

Herwegh, M. & Pfiffner, O. A. (2005). Tectono-metamorphic evolution of a nappe stack: A case study of the Swiss Alps. *Tectonophysics, 404*, 55-76. https://doi.org/10.1016/j.tecto.2005.05.002

Herwegh, M., Berger, A., Glotzbach, C., Wangenheim, S., Mock, S., Wehrens, P., Baumberger, R., Egli, D. & Kissling, E. (2020). Late stages of continent-continent collision: Timing, kinematic, evolution and exhumation of the Northern rim (Aar Massif)

of the Alps. *Earth-Science Reviews, 200*, 102959. https://doi.org/10.1016/j.earscirev.2019.102959

Jammes, S., Manatschal, G., Lavier, L. & Masini, E. (2009). Tectonosedimentary evolution related to extreme crustal thinning ahead of a propagating ocean: Example of the western Pyrenees. *Tectonics, 28*, 1-24. https://doi.org/10.1029/2008TC002406

Jolivet, M., Labaume, P., Monié, P., Brunel, M., Arnaud, N. & Campani, M. (2007). Thermochronology constraints for the propagation sequence of the south Pyrenean basement thrust system (France-Spain). *Tectonics, 26 (5)*, 1-17. https://doi.org/10.1029/2006TC002080

Labaume, P., Meresse, F., Jolivet, M., Teixell, A. & Lahfid, A. (2016). Tectonothermal history of an exhumed thrust-sheet-top basin: An example from the south Pyrenean thrust belt. *Tectonics, 35*, 1280-1313. https://doi.org/10.1002/2016TC004192

Labaume, P. & Teixell, A. (2020). Evolution of salt structures of the Pyrenean rift (Chaînons Béarnais, France): From hyper-extension to tectonic inversion. *Tectonophysics, 785*, 228451. https://doi.org/10.1016/j.tecto.2020.228451

Lacombe, O. & Bellahsen, N. (2016). Thick-skinned tectonics and basement-involved fold-thrust belts: Insights from selected Cenozoic orogens. *Geological Magazine, 153*, 763-810. https://doi.org/10.1017/S0016756816000078

Lagabrielle, Y., Labaume, P. & de Saint Blanquat, M. (2010). Mantle exhumation, crustal denudation, and gravity tectonics during Cretaceous rifting in the Pyrenean realm (SW Europe): Insights from the geological setting of the lherzolite bodies. *Tectonics, 29*, 1-26. https://doi.org/10.1029/2009TC002588

Lahfid, A., Beyssac, O., Deville, E., Negro, F., Chopin, C. & Goffé, B. (2010). Evolution of the Raman spectrum of carbonaceous material in low-grade metasediments of the Glarus Alps (Switzerland). *Terra Nova, 22*. 354-360. https://doi.org/10.1111/j.1365-3121.2010.00956.x

Majesté-Menjoulas, C. (1979). Evolution alpine d'un segment de la chaîne varisque. Nappe de Gavarnie, chevauchements Cinq-Monts-Gentiane (Pyrénées centrales et occidentales). *Thesis Université of Toulouse,* 343 p.

Masini, E., Manatschal, G., Tugend, J., Mohn, G. & Flament, J.-M. (2014). The tectono-sedimentary evolution of a hyper-extended rift basin: The example of the Arzacq-Mauléon rift system (Western Pyrenees, SW France). *International Journal of Earth Sciences, 103*, 1569-1596. https://doi.org/10.1007/s00531-014-1023-8

Metcalf, J. R., Fitzgerald, P. G., Baldwin, S.L. & Muñoz, J. A. (2009). Thermochronology of a convergent orogen: Constraints on the timing of thrust faulting and subsequent exhumation of the Maladeta Pluton in the Central Pyrenean Axial Zone. *Earth and Planetary Science Letters, 287 (3-4)*, 488-503. https://doi.org/10.1016/j.epsl.2009.08.036

Mouthereau, F., Filleaudeau, P.-Y., Vacherat, A., Pik, R., Lacombe, O., Fellin, M. G., Castelltort, S., Christophoul, F. & Masini, E. (2014). Placing limits to shortening evolution in the Pyrenees: Role of margin architecture and implications for the Iberia/Europe convergence. *Tectonics, 33*, 2283-2314. https://doi.org/10.1002/2014TC003663

Muñoz, J. A. (1992). Evolution of a continental collision belt: ECORS-Pyrenees crustal balanced cross-section. *Thrust Tectonics*, 235-246. https://doi.org/10.1007/978-94-011-3066-0_21

Nemanich, R. J. & Solin, S. A. (1979). First- and second-order Raman scattering from finite-size crystals of graphite. *Physical Review B, 20*, 392-401. https://doi.org/10.1103/PhysRevB.20.392

Nibourel, L., Berger, A., Egli, D., Luensdorf, N. K. & Herwegh, M. (2018). Large vertical displacements of a crystalline massif recorded by Raman thermometry. *Geology, 46*, 879-882. https://doi.org/10.1130/G45121.1

Pfiffner, O. A. (1993). The structure of the Helvetic nappes and its relation to the mechanical stratigraphy. *Journal of Structural Geology, 15*, 511-521. https://doi.org/10.1016/0191-8141(93)90145-Z

Pfiffner, O. A., Lehner, P., Heitzmann, P., Mueller, St. & Steck, A. (1997). Deep Structure of the Swiss Alps: Results from NFP 20. *Birkhäuser Verlag, Basel, Switzerland,* 460pp. ISBN 3-7643 5254 X, Hardback, DM 228.

Pfiffner, O. A. (2017). Thick-skinned and thin-skinned tectonics: A global perspective. *Geosciences, 7 (3)*, 71. https://doi.org/10.3390/geosciences7030071

Ramsay, J. G. (1981). Tectonics of the Helvetic nappes. *Geological Society, London, Special Publications, 9*, 293-309. https://doi.org/10.1144/GSL.SP.1981.009.01.26

Saspiturry, N., Lahfid, A., Baudin, T., Guillou-Frottier, L., Razin, P., Issautier, B., Le Bayon, B., Serrano, O., Lagabrielle, Y & Corre, B. (2020). Paleogeothermal Gradients Across an Inverted Hyperextended Rift System: Example of the Mauléon Fossil Rift (Western Pyrenees). *Tectonics, 39*. https://doi.org/10.1029/2020TC006206

Souquet, P. (1967). Le Crétacé supérieur sudpyrénéen en Catalogne, Aragon et Navarre. *Thèse d'Etat, Université de Toulouse*, 529 p.

Stipp, M., Stünitz, H., Heilbronner, R. & Schmid, S. M. (2002). Dynamic recrystallization of quartz: Correlation between natural and experimental conditions. Geological Society of London, Special Publications, 200 (1), 171-190. https://doi.org/10.1144/GSL.SP.2001.200.01.11

Teixell, A. (1993). Coupe géologique du massif d'Igountze: implications sur l'évolution structurale de la bordure sud de la Zone nord-pyrénéenne occidentale. *Comptes Rendus de l'Académie des Sciences, Paris, 316*, 1789-1796.

Teixell, A., García Sansegundo, J., & Zamorano, M. (1994). Memoria de la Hoja nº 144 (Anso). *Mapa Geológico de España E. 1:50.000 (MAGNA),* Segunda Serie, Primera edición. IGME, 62 p.

Teixell, A. (1996). The Ansó transect of the southern Pyrenees: Basement and cover thrust geometries. *Journal of the Geological Society of London, 153*, 301-310. https://doi.org/10.1144/gsjgs.153.2.0301

Teixell, A. (1998). Crustal structure and orogenic material budget in the west central Pyrenees. *Tectonics, 17 (3)*, 395-406. https://doi.org/10.1029/98TC00561

Teixell, A., Labaume, P. & Lagabrielle, Y. (2016). The crustal evolution of the west-central Pyrenees revisited: Inferences from a new kinematic scenario. *Comptes Rendus – Geoscience, 348*, 257-267. https://doi.org/10.1016/j.crte.2015.10.010

Teixell, A., Labaume, P., Ayarza, P., Espurt, N., de Saint Blanquart, M. & Lagabrielle, Y. (2018). Crustal structure and evolution of the Pyrenean-Cantabrian belt: A review and

new interpretations from recent concepts and data. *Tectonophysics, 724-725*, 149-170. https://doi.org/10.1016/j.tecto.2018.01.009

Ternet, Y. (1965). Étude du synclinal complexe des Eaux-Chaudes (Basses-Pyrénées), *Thèse Doctorat 3º Cycle: Faculté des sciences de l'Université de Toulouse*, 332 p.

Ternet, Y., Majeste-Menjoulas, C., Canerot, J., Baudin, T., Cocherie, A., Guerrot, C. & Rossi, P. (2004). *Carte géologique de la France:* Laruns-Somport. Bureau de Recherches Géologiques et Minières, scale 1:50.000, feuille nº1069.

Tuinstra, F. & Koenig, J. L. (1970). Raman Spectrum of Graphite. *The Journal of Chemical Physics, 53*, 1126-1130. https://doi.org/10.1063/1.1674108

Weber, J. C., Ferrill, D. A. & Roden-Tice M. K. (2001). Calcite and quartz microestructural geothermometry of low-grade metasedimentary rocks, Northern Range, Trinidad. *Journal of Structural Geology, 23 (1)*, 93-112. https://doi.org/10.1016/S0191-8141(00)00066-3

Figure captions

FIGURE 1. (A) Geologic sketch map of the Pyrenees showing the location of the Eaux-Chaudes massif. White frame indicates the mapped area (Fig. 2) and white line indicates cross-section in Figure 1B. (B) Crustal cross-section of the Pyrenees west of the study zone (simplified from Teixell et al., 2016) showing the tectonic setting of the: Eaux-Chaudes structure (red frame); CBB: Chaînons Béarnais Belt; IM: Igountze Mendibelza; GT: Gavarnie thrust; LT: Lakora thrust; NPZ: North-Pyrenean Zone; NPF: North-Pyrenean fault; NPFT: North-Pyrenean Frontal thrust; SPZ: South-Pyrenean Zone; SPFT: South-Pyrenean Frontal Thrust.

FIGURE 2. (A) Geological map of the Chaînons Béarnais belt (North-Pyrenean Zone) and Eaux-Chaudes massif, location in Figure 1a; NPF: North-Pyrenean fault. Modified from Labaume & Teixell (2020). (B) Detailed geological map of the study area in the Ossau Valley, western Eaux-Chaudes massif (location in Fig. 2b). Data compiled from published maps (Ternet, 1965; Ternet et al., 2004), completed with additional own field studies. White line indicates cross-section in Figure 3.

FIGURE 3. Cross-section of the recumbent Eaux-Chaudes fold nappe in the western side of the Ossau valley (see Fig. 2b for location).

FIGURE 4. Outcrop photo and interpreted profile of the Eaux-Chaudes nappe structure at the western side of the Ossau valley (see Fig. 2b for location). Gray arrows indicate bedding polarity. Colour codes correspond to those given in Figure 3.

FIGURE 5. (A) Equal area upper hemisphere pole figures of calcite a-, m- and c-axes measured by EBSD for the undeformed Upper Cretaceous limestone from the normal limb of the Eaux-Chaudes fold nappe (sample 17NC51, cut perpendicular to bedding), showing random crystallographic orientation. (B) Band contrast image and Inverse Pole Figure (IPF) map for sample 17NC51. (C) Stereonet reference frame with xyz spatial axes for deformed samples of the overturned limb. Pole figures and images correspond to the xz plane. (D) Equal area upper hemisphere pole figures of calcite a-, m- and c-axes fabrics deformed of sample 17NC26, showing a moderate crystallographic preferred orientation. (E) Band contrast image and IPF map of sample 17NC26 showing S-C composite structure. (See Fig. 2b and table 1 for sample location).

FIGURE 6. Deformed samples from the overturned limb at the locality of Cambeilh (see Fig. 2 for location). Arrows indicate the shear direction. (A) Asymmetric dolomite porphyroclasts in a dark recrystallized calcite matrix. (B) Intramylonitic folds (dashed white lines) in sheared limestone. (C) Stretching lineation (dashed white lines) on the mylonitic foliation planes. All of these structures indicate top to the south sense of tectonic transport. (D), (E); Stereographic projection of (D) main foliation and (E) stretching lineation measured in the Upper Cretaceous rocks. (lower hemisphere, equal area).

FIGURE 7. Representative Raman spectra of carbonaceous material and photomicrographs of three samples from the Upper Cretaceous rocks, in a vertical profile across the Eaux-Chaudes fold nappe. (A) Undeformed sample from the normal limb of the recumbent fold. (B) Deformed sample from the overturned limb of the recumbent fold. (C) Undeformed sample from the autochthon (see Fig. 2b and table 1 for sample location).

FIGURE 8. Cartoon (not to scale) illustrating the development and evolution of the Eaux-Chaudes recumbent fold during the D1 stage of the Pyrenean compressional deformation. Thickness of Upper Triassic and subsequent units are poorly constrained. Relicts of Upper Triassic rocks (Keuper and

ophites) between the overturned limb and autochthon remain from its extrusion while the fold nappe progressively evolved.

TABLE 1. Summary of samples used in Raman and EBSD study. Zone indicates the structural position of samples (Au: Autochthonous; OL: Overturned Limb; NL: Normal Limb). *RA1* and *RA2* values were retrieved from peak-fitting of Raman spectra (mean and standard deviation). *RA1*, (D1+D4)/(D1+D2+D3+D4+G); *RA2*, (D1+D4)/(D2+D3+G); Maximum temperatures were estimated after the methods by Beyssac et al. (2002) and Lahfid et al. (2010). Asterisks indicate EBSD analysed samples.

TABLE 1. RESULTS OF RSCM

Sample	Latitude N	Longitude W	Zone	R2 parameter		RA1 parameter		Number of spectra	T (ºC)	SD
				Mean	SD	Mean	SD		Mean	
17NC21	42º 56'44.69''	0 º 26' 39.45''	Au	0.67	0.03	-	-	17	340	8
17NC26*	42º 58'3.27''	0 º 26' 20.03''	OL	0.65	0.02	-	-	16	348	8
17NC27*	42º 58'14.39''	0 º 26' 17.28''	OL	0.64	0.02	-	-	22	355	7
17NC34*	42º 55'52.68''	0 º 25' 52.96''	OL	0.66	0.02	-	-	21	344	6
17NC37*	42º 56'7.22''	0 º 25' 22.92''	OL	0.68	0.02	-	-	18	337	8
18NC04	42º 56'2.59''	0 º 27' 7.40''	OL	0.68	0.03	-	-	15	334	7
18NC46	42º 57'19.84''	0 º 29' 21.50''	NL	0.70	0.01	-	-	15	328	5
18NC47	42º 57'17.08''	0 º 29' 21.61''	NL	0.72	0.01	-	-	12	321	4
18NC16	42º 58'5.81''	0 º 29' 36.55''	NL	-	-	0.62	0.01	14	311	10
18NC17	42º 58'6.62''	0 º 29' 37.71''	NL	-	-	0.63	0.01	10	316	15
18NC20	42º 58'0.87''	0 º 29' 34.21''	NL	-	-	0.63	0.01	14	317	11
18NC37	42º 57'46.53''	0 º 29' 37.65''	NL	-	-	0.63	0.01	10	313	15
18NC48	42º 57'5.41''	0 º 29' 17.86''	NL	-	-	0.63	0.01	12	315	13
17NC51*	42º 59'13.80''	0 º 30' 27.30''	NL	-	-	-	-	-	-	-

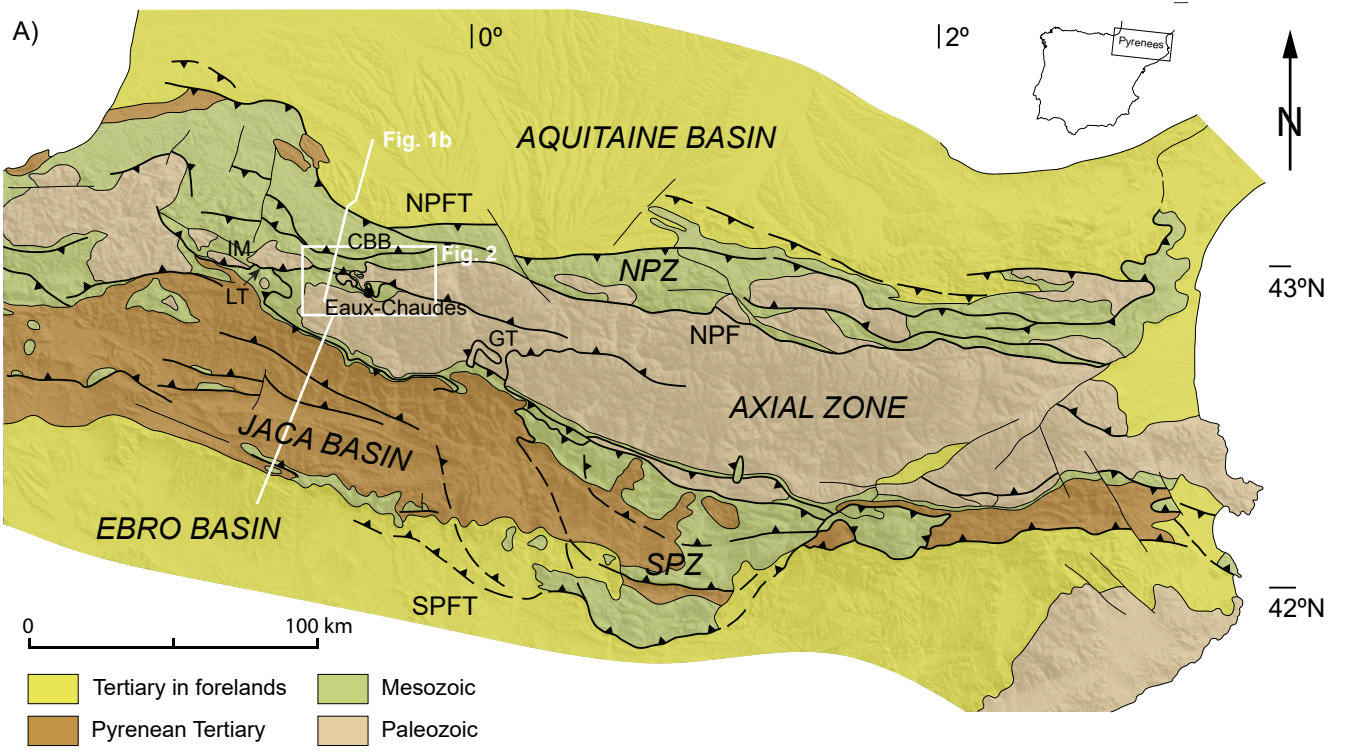
A)
0º
2º
Pyrenees
N
Fig. 1b
AQUITAINE BASIN
NPFT
IM
CBB
Fig. 2
LT
Eaux-Chaudes
NPZ
GT
NPF
43ºN
AXIAL ZONE
JACA BASIN
EBRO BASIN
SPZ
SPFT
42ºN
0
100 km
Tertiary in forelands
Mesozoic
Pyrenean Tertiary
Paleozoic

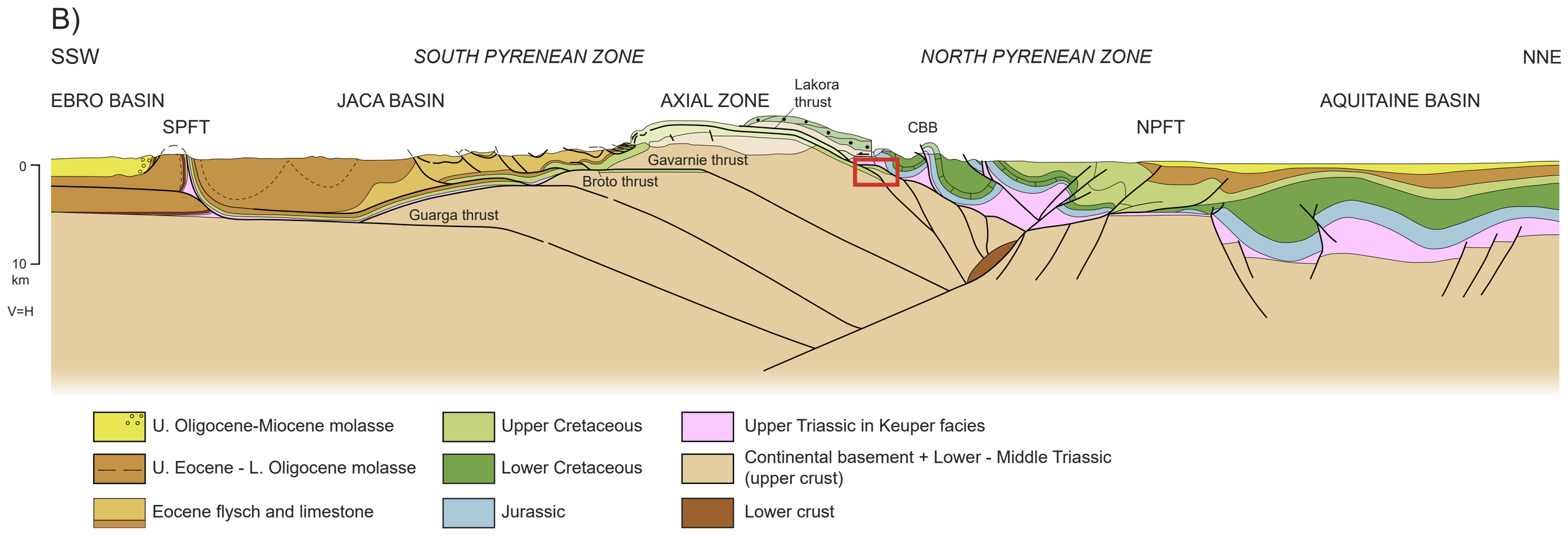
B)
SSW
SOUTH PYRENEAN ZONE
NORTH PYRENEAN ZONE
NNE
EBRO BASIN
JACA BASIN
AXIAL ZONE
Lakora thrust
AQUITAINE BASIN
SPFT
CBB
NPFT
Gavarnie thrust
Broto thrust
Guarga thrust
0
10
km
V=H
U. Oligocene-Miocene molasse
U. Eocene - L. Oligocene molasse
Eocene flysch and limestone
Upper Cretaceous
Lower Cretaceous
Jurassic
Upper Triassic in Keuper facies
Continental basement + Lower - Middle Triassic (upper crust)
Lower crust

A)

W0°40'
W0°30'
W0°20'
N43°00'
Mail Arrouy
Sarrance
CHAINONS BEARNAIS
LICQ FAULT
Iguntze
Layens
Bedous
OUZOM
NPF
Arbéost
Laruns
BEDOUS - LARUNS THRUST UNITS
LAKORA Th.
Bergon
Montagnon
Iseye
EAUX-CHAUDES Th.
Eaux-Chaudes massif
EAUX-BONNES Th.
Gave d'ASPE
Fig. 2b
AXIAL ZONE
Eaux-Chaudes granite
Gave d'OSSAU
N
5 km

Campanian-Maastrichtian (flysch)

Cenomanian to Santonian (south: carbonates ; north: flysch)

Upper Aptian to lower Cenomanian (Spicule marls and Black Flysch Group) (Iguntze: Mendibelza conglomerates; Arbéost, Bazès and Gallagos: mainly carbonates)

Jurassic to lower Albian carbonates

Middle-Upper Triassic (Keuper facies, Muschelkalk carbonates and ophite)

a) Paleozoic metasediments and Lower Triassic sandstone
b) Late Variscan granitoids

Lherzolite

Upper Cretaceous alkaline magmatic rocks (intrusive sheets and pillow lavas)

Detachment contact

Thrust fault

Thrust on reactivated diapir/weld

Welded diapir

Normal fault

Undifferentiated fault or diapir contact

B)

0°27'W

42°55'N

Laruns

Montagnon d'Iseye

Pic de Bouerzy

Goust

Les Eaux-Chaudes

Pic du Gourzy

Cabane du Cambeilh

Pic de Cézy

Ossau Valley

17NC51

18NC16

18NC17

18NC20

18NC37

18NC46

18NC47

18NC48

17NC27

17NC26

17NC21

18NC04

17NC37

17NC34

Figs. 3 - 4

N

1 km

Quaternary
Campanian - Maastrichtian
Coniacian - Santonian
Cenomanian - Turonian
Keuper and ophites
Buntsandstein
Eaux-Chaudes granite
Carboniferous
Upper Devonian
Lower Devonian
Silurian
Detachment contact
Thrust fault
Welded contact
Indiferentiated fault
Sample location

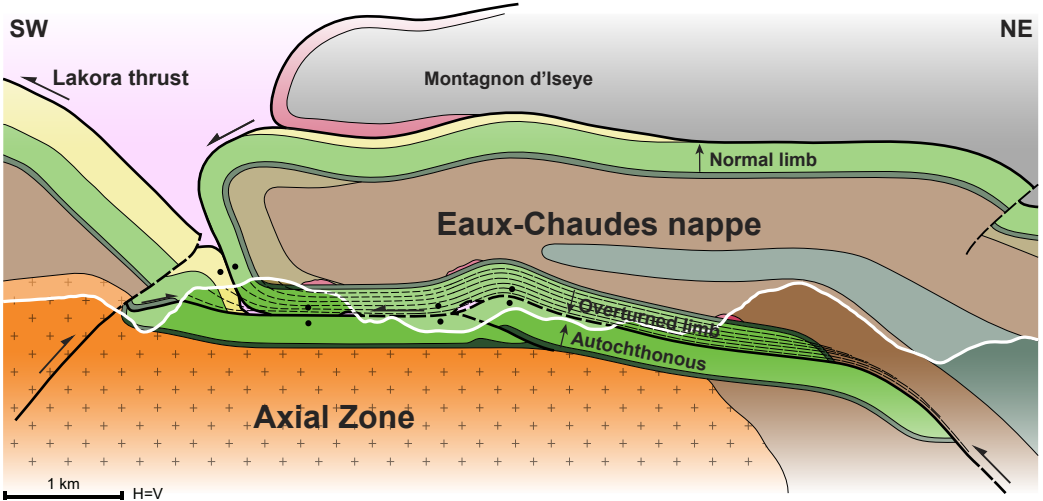
SW
NE
Lakora thrust
Montagnon d'Iseye
Normal limb
Eaux-Chaudes nappe
Overturned limb
Autochthonous
Axial Zone
1 km
H=V
Campanian - Maastrichtian
Coniacian - Santonian
Cenomanian - Turonian
Keuper and ophites
Buntsandstein
Eaux-Chaudes granite
Carboniferous
Upper Devonian
Lower Devonian
Silurian
Welded contact

Montagnon d'Iseye

Goust

S

N

Lakora thrust

Axial Zone

Eaux-Chaudes nappe

1 Km

A) **17NC51**

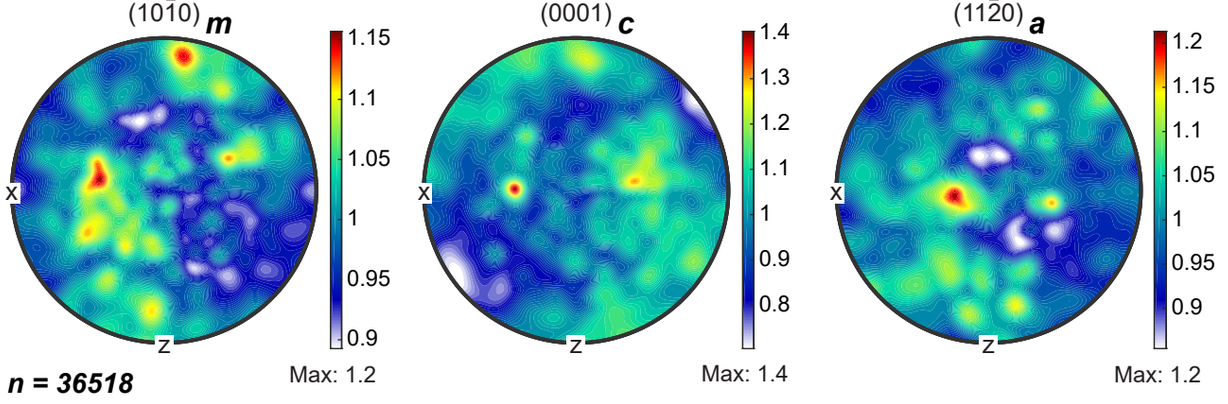

n = 36518

Max: 1.2 Max: 1.4 Max: 1.2

B)

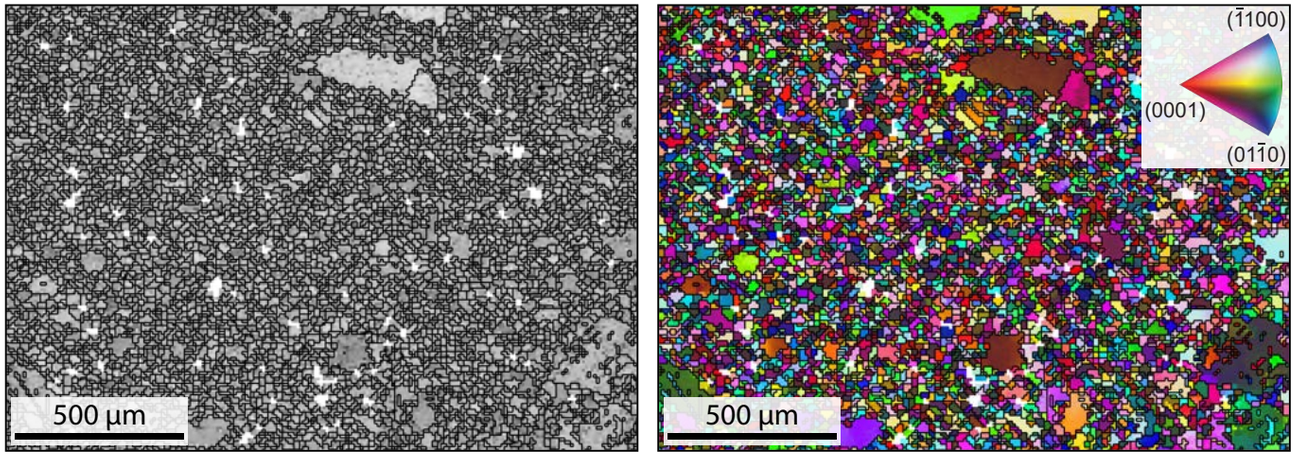

C) Stereonet reference frame

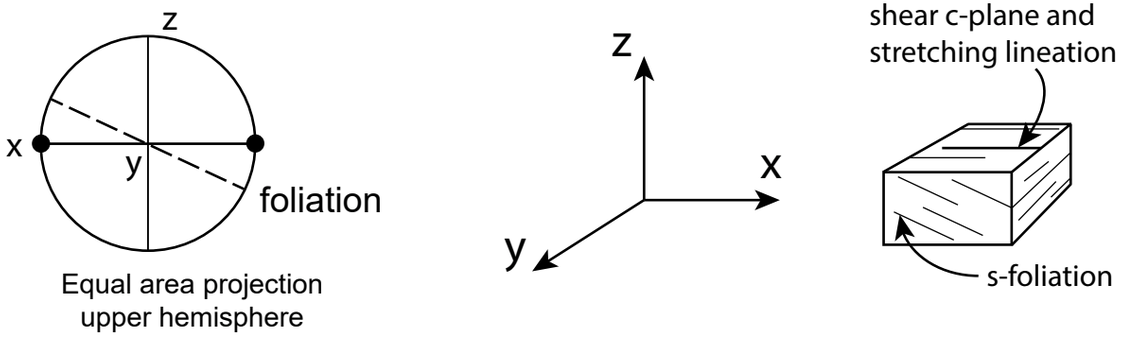

D) **17NC26**

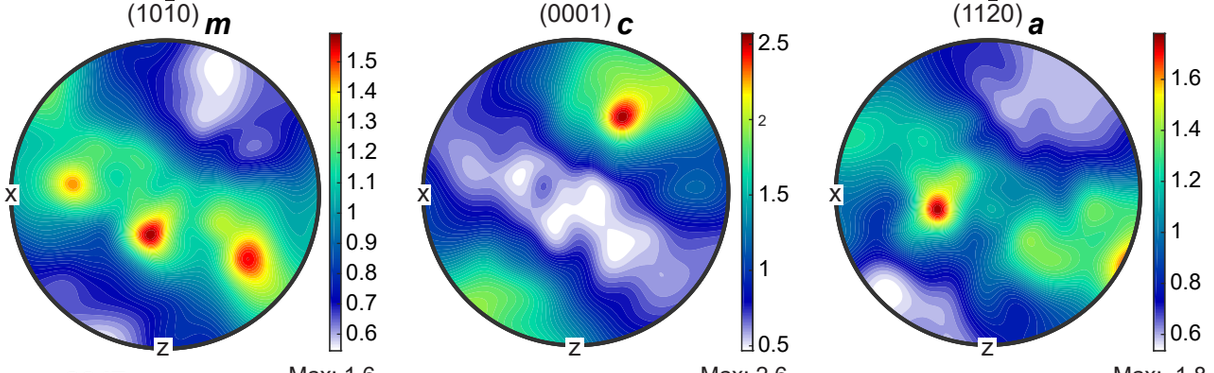

n = 8647

Max: 1.6 Max: 2.6 Max: 1.8

E)

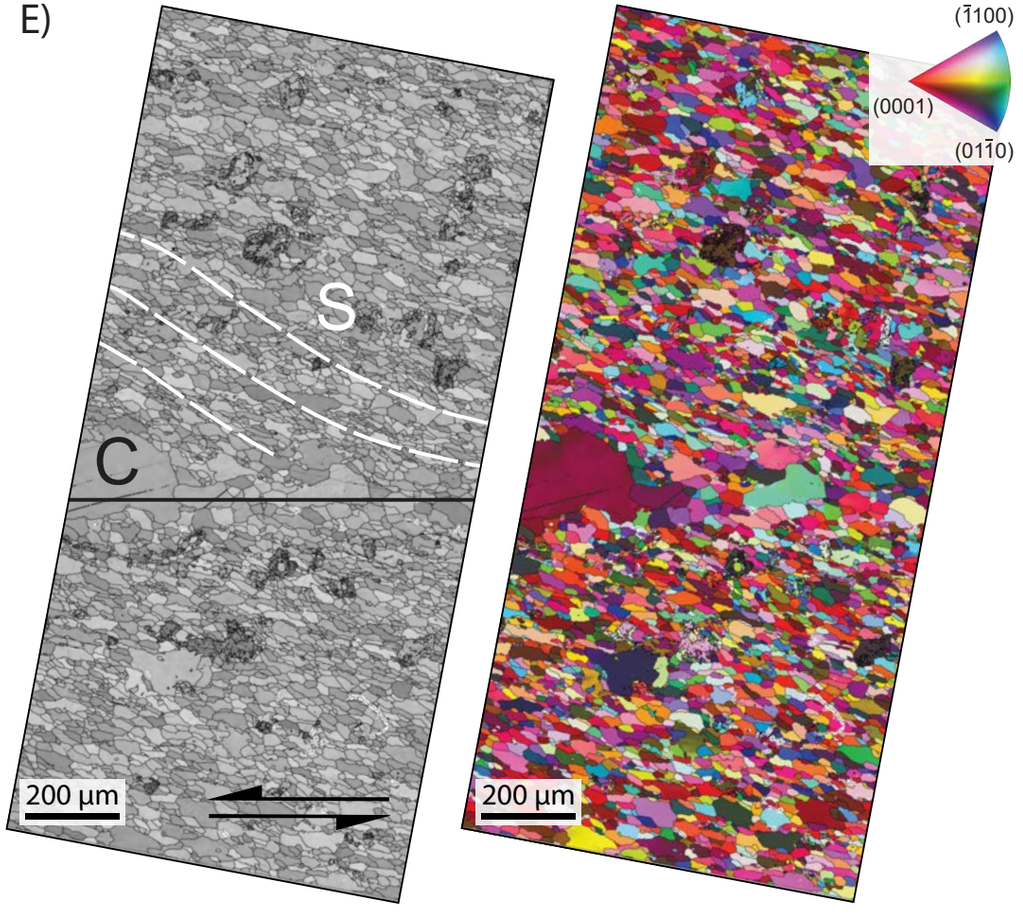

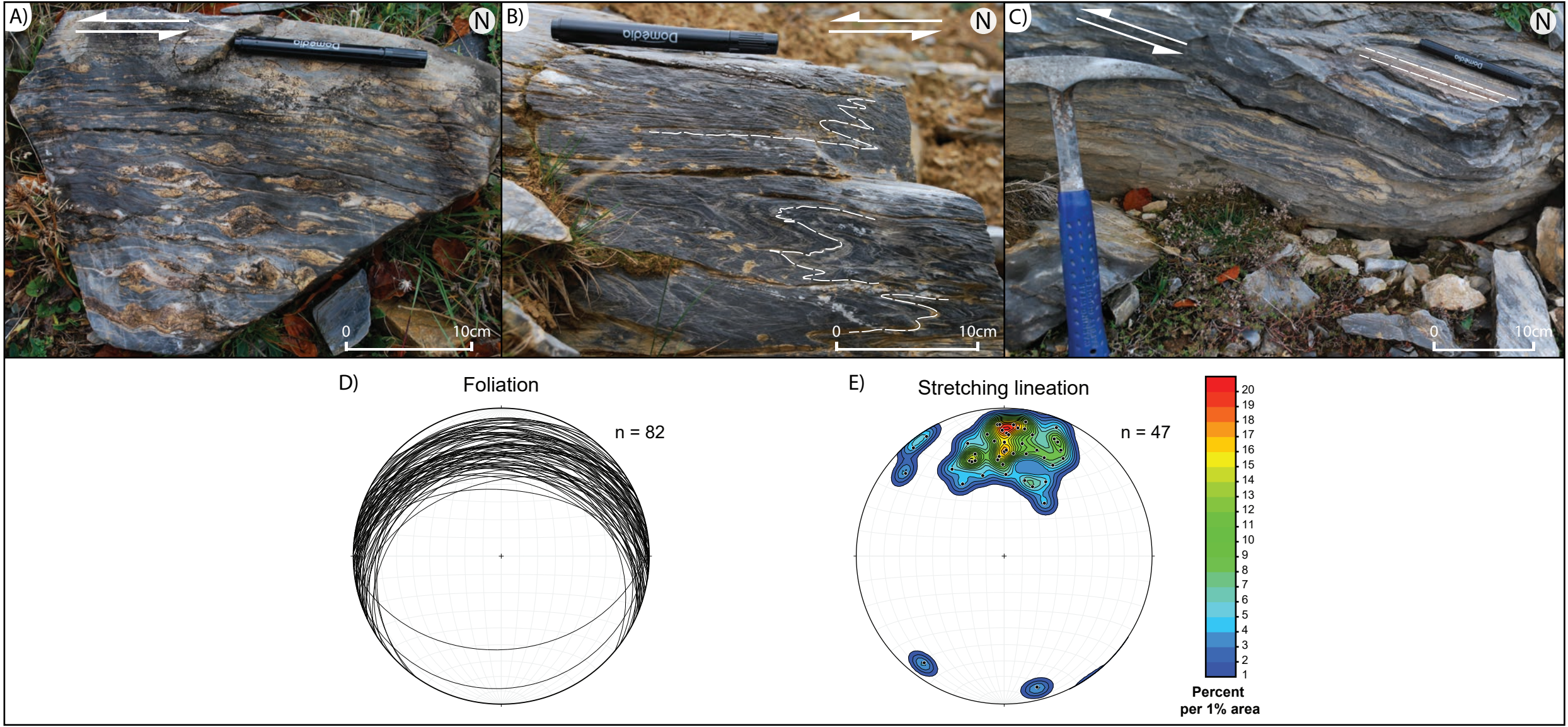
A)
N
0
10cm
B)
N
0
10cm
C)
N
0
10cm
D)
Foliation
n = 82
E)
Stretching lineation
n = 47
20
19
18
17
16
15
14
13
12
11
10
9
8
7
6
5
4
3
2
1
Percent
per 1% area

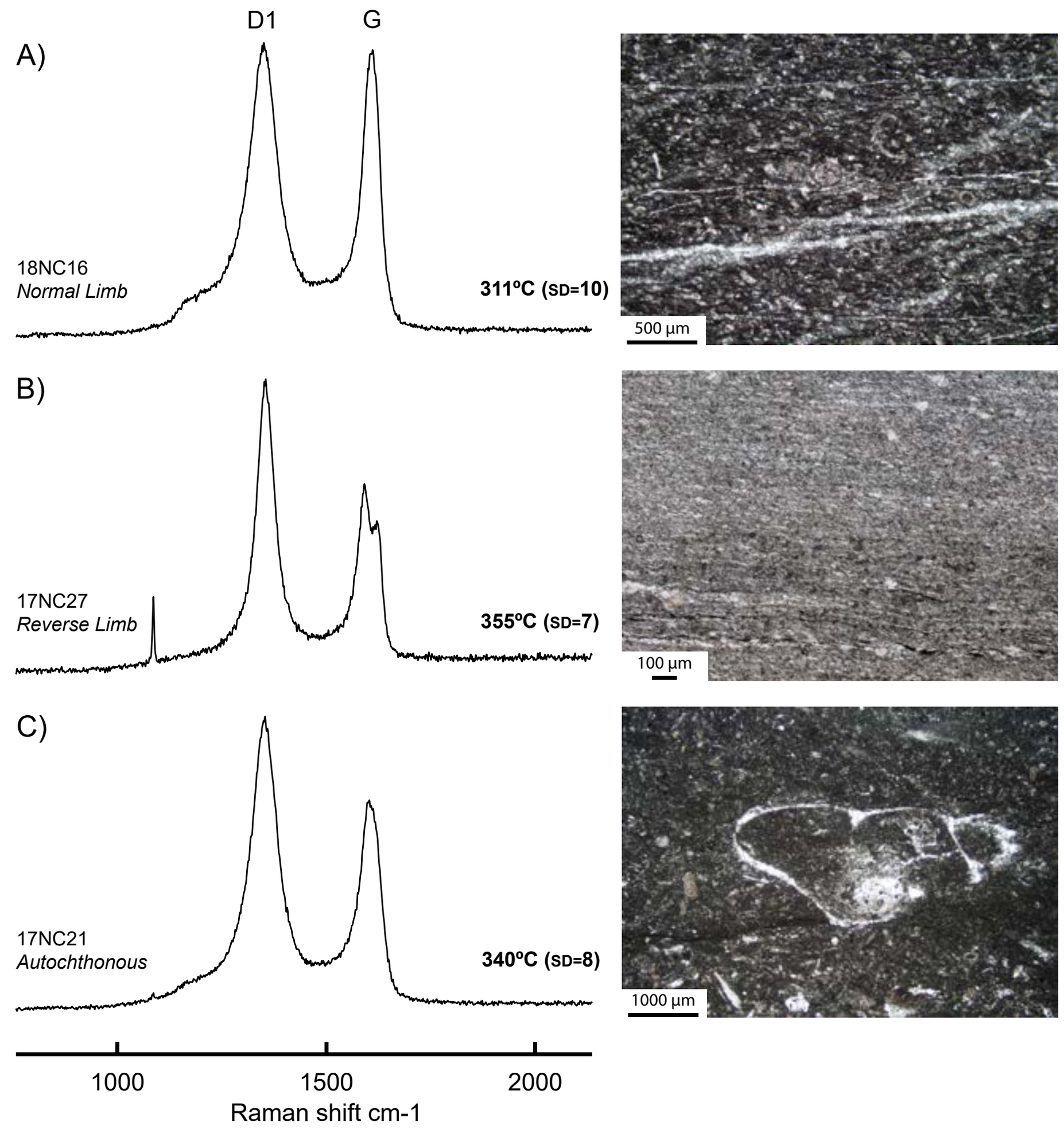
D1
G
A)
18NC16
Normal Limb
311ºC (SD=10)
500 µm
B)
17NC27
Reverse Limb
355ºC (SD=7)
100 µm
C)
17NC21
Autochthonous
340ºC (SD=8)
1000 µm
1000
1500
2000
Raman shift cm-1

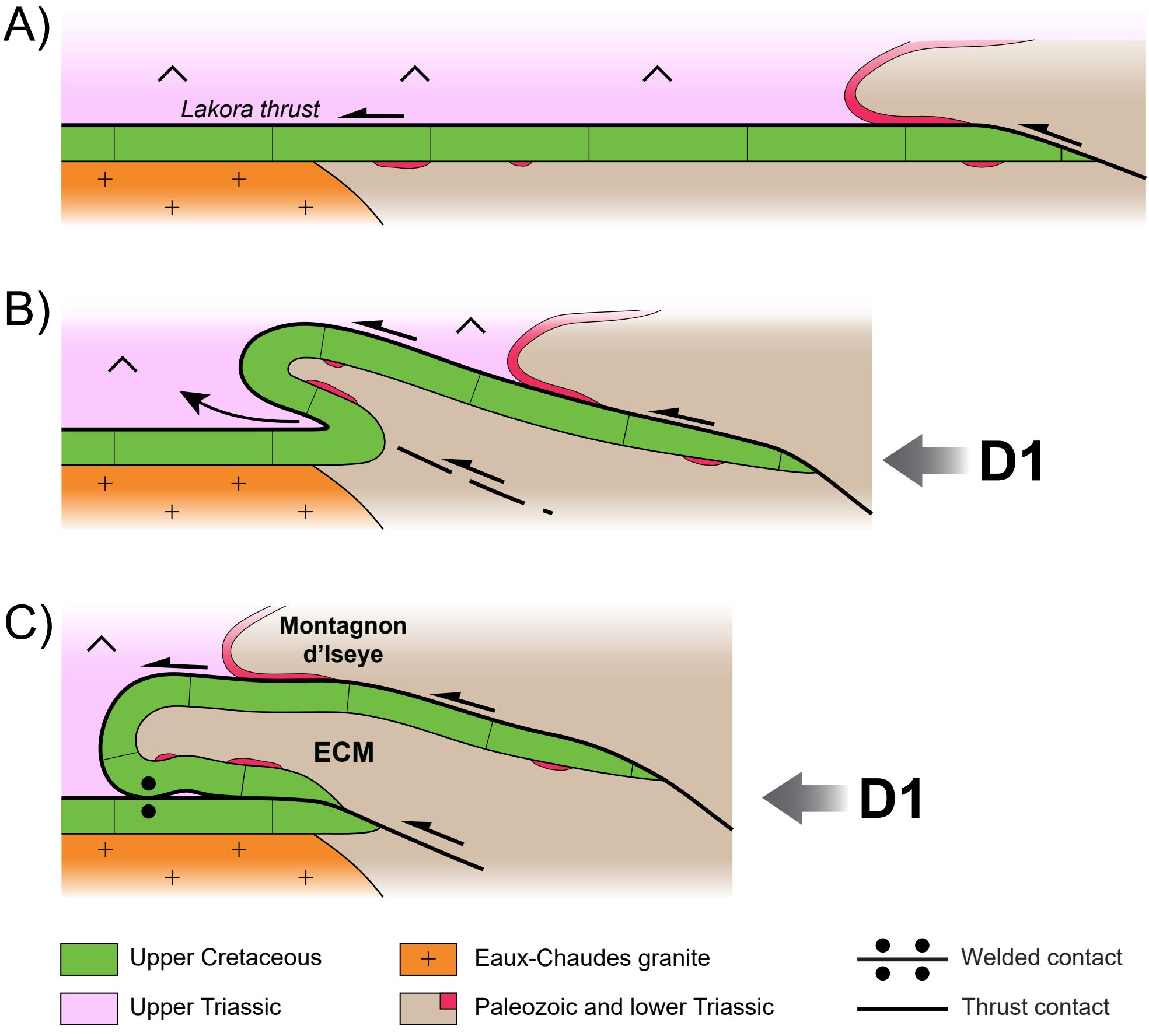
A)
Lakora thrust
B)
D1
C)
Montagnon
d'Iseye
ECM
D1
Upper Cretaceous
Upper Triassic
Eaux-Chaudes granite
Paleozoic and lower Triassic
Welded contact
Thrust contact